HHS Public Access

Author manuscript

Nature. Author manuscript; available in PMC 2015 March 24.

Published in final edited form as:

Nature. 2004 November 4; 432(7013): 59–67. doi:10.1038/nature02976.

Structural basis for allostery in integrins and binding to fibrinogen-mimetic therapeutics

Tsan Xiao[1], **Junichi Takagi**[1,*], **Barry S. Coller**[2], **Jia-Huai Wang**[3], and **Timothy A. Springer**[1]

[1]The CBR Institute for Biomedical Research and Department of Pathology, Harvard Medical School, 200 Longwood Avenue, Boston, Massachusetts 02115, USA

[2]Laboratory of Blood and Vascular Biology, The Rockefeller University, 1230 York Avenue, New York, New York 10021, USA

[3]Dana-Farber Cancer Institute, Departments of Pediatrics, Biological Chemistry and Molecular Pharmacology, Harvard Medical School, 44 Binney Street, Boston, Massachusetts 02115, USA

Abstract

Integrins are important adhesion receptors in all Metazoa that transmit conformational change bidirectionally across the membrane. Integrin α and β subunits form a head and two long legs in the ectodomain and span the membrane. Here, we define with crystal structures the atomic basis for allosteric regulation of the conformation and affinity for ligand of the integrin ectodomain, and how fibrinogen-mimetic therapeutics bind to platelet integrin $\alpha_{IIb}b_{\beta3}$. Allostery in the β_3 I domain alters three metal binding sites, associated loops and a α1- and α7-helices. Piston-like displacement of the a 7-helix causes a 62° reorientation between the β_3 I and hybrid domains. Transmission through the rigidly connected plexin/semaphorin/integrin (PSI) domain in the upper β_3 leg causes a 70Å separation between the knees of the α and β legs. Allostery in the head thus disrupts interaction between the legs in a previously described low-affinity bent integrin conformation, and leg extension positions the high-affinity head far above the cell surface.

Integrins are adhesion receptors that transmit signals bidirectionally across the plasma membrane[1–4]. Rearrangements in integrin extracellular, transmembrane and cytoplasmic domains underlie diverse biological processes, including cell migration, morpho-genesis, immune responses and vascular haemostasis. The platelet-specific integrin $\alpha_{IIb}\beta_3$ is important in both the arrest of bleeding at sites of vascular injury and pathological thrombosis leading to heart attacks and stroke. Loss of the vascular endothelium results in platelet deposition, and receptors for collagen, thrombin and other agonists then initiate

Correspondence and requests for materials should be addressed to T.A.S. (springer@cbr.med.harvard.edu)..

*Present address: Institute for Protein Research, Osaka University, 3-2 Yamadaoka, Suita, Osaka 565-0871, Japan

Atomic coordinates and structural factors have been deposited with the Protein Data Bank with the accession codes 1TY3 (form A + cacodylate 1); 1TXV (form A + cacodylate 2); 1TY5 (form A + tirofiban); 1TY6 (form A + eptifibatide); 1TY7 (form A + L-739758); 1TYE (form B + cacodylate). Sequences of the with GenBank.

Supplementary Information accompanies the paper on **www.nature.com/nature**.

Competing interests statement The authors declare competing financial interests: details accompany the paper on **www.nature.com/nature**.

platelet signalling, resulting in changes in the cytoplasmic domains of $\alpha_{IIb}\beta3$ that are transmitted into conformational changes in the extracellular domains. This leads to high-affinity binding of fibrinogen and von Willebrand factor, resulting in crosslinking of platelets into aggregates by these multivalent ligands, and activation by $\alpha_{IIb}\beta3$ of further intracellular signals. Mutations of either α_{iib} or β_3 result in the bleeding disorder Glanzmann thrombasthenia and drugs that inhibit ligand binding to $\alpha_{IIb}\beta3$ are effective in preventing and treating coronary artery thrombosis[5].

Global structural rearrangements in integrin extracellular domains are demonstrated by electron microscopy and exposure of activation epitopes known as ligand-induced binding sites (LIBS)[2,4]. Negative stain electron microscopy with image averaging of integrins has demonstrated three overall conformations of the extracellular domain[3,6] (Fig. 1a–c). A low-affinity, bent conformation (Fig. 1a) matches $\alpha_V\beta_3$ crystal structure[7,8]. An extended form with a 'closed' headpiece conformation matching that in the crystal structure represents an intermediate affinity state (Fig. 1b). Ligand-binding induces a high-affinity, extended form with an 'open' headpiece, in which the angle between the β I and hybrid domains changes from acute to obtuse[3,6] (Fig. 1c). This marked change in tertiary structure is supported by mutational studies[3,6,9–11] and solution X-ray scattering[12]. Ligand-mimetic compounds induce the extended, open headpiece conformation of integrins in solution and on the cell surface[3,6,10–13], and LIBS epitope exposure[14]. In contrast, when a ligand-mimetic is soaked into preformed crystals containing the bent integrin conformation with the closed headpiece, binding induces only localized structural changes near the ligand binding site[8].

In the low-affinity bent structure, the α and β subunit ecto-domain carboxy termini[7] and transmembrane domains are closely associated[15,16], and transmission of activation signals across the membrane involves separation between the α and β transmembrane and cytoplasmic domains[16–18]. How allostery could be relayed between the integrin transmembrane domains, legs and ligand-binding head has been unclear. We have proposed that the conformation of the ligand-binding site atop the integrin β I domain could be transmitted to the outward swing of the β hybrid domain between the closed and open headpiece conformations (Fig. 1b, c) by a piston-like β I domain α7-helix motion similar to that seen in integrina βI domains[3,6]. However, in the absence of atomic views of the high-affinity integrin state, different opinions about its conformation have been put forward.

Here, atomic structures of $\alpha_{IIb}\beta3$ fragments demonstrate the high-affinity, open conformation of the integrin headpiece, its binding to therapeutic antagonists, and the allosteric movements that link the ligand binding site of βI domains to α7-helix displacement and outward swing of the hybrid domain. The β_3 hybrid and PSI domains act as a rigid lever that transmits and amplifies this motion, resulting in a 70Å separation between the α and β legs at their knees that favours leg extension.

Overall structure of an open integrin headpiece

Two crystal forms each contain α_{iib} residues 1–452 comprising the yyβ-propeller domain and β_3 residues 1–440 including the β I, hybrid and PSI domains (Fig. 2a, b and Supplementary Table 1). Crystal form A contains one copy per asymmetric unit of the

$\alpha_{IIb}\beta 3$ headpiece bound to 10E5 Fab[19] (Fig. 2a), and ligand-mimetic antagonist or cacodylate ion bound to the β_3 I domain metal-ion-dependent adhesion site (MIDAS) (2.7–3.1Å resolution). Crystal form B contains no Fab and three independent, cacodylate-bound $\alpha_{IIb}\beta 3$ molecules per asymmetric unit (2.9Å resolution). The four independent $\alpha_{IIb}\beta 3$ headpiece fragments from the two crystal forms adopt similar conformations, with only minor differences in the angle between the β I and hybrid domains (Fig. 2b). Five N-linked glycans are resolved, including one in a form A crystal lattice contact with seven carbohydrate residues (Fig. 2a). Residues 55–77 in our β_3 hybrid domain structures have a different sequence-structure register than previousβ_3 structures (Supplementary Material).

Our crystal structures reveal an open, high-affinity conformation of the $\alpha_{IIb}\beta 3$ headpiece similar to that in electron microscopy averages of the $\alpha_V\beta_3$ ectodomain in which ligand binding induced the extended conformation with the open headpiece[3] (Fig. 1c). Relative to the bent $a_V\beta_3$ crystal structure with the closed, lowaffinity conformation of the headpiece[3,7], the α7-helix of the β_3 I domain moves downward, causing the hybrid and PSI domains to swing away from the α subunit by 62° (Fig. 2d). The angle between the β I and hybrid domains visualized here is in excellent agreement with that found by electron microscopy for liganded$a_V\beta_3$ (ref. 3) and the α_5b_1 headpiece bound to FN3 module 10 of fibronectin[6] (Fig. 2e). Ligand-mimetic antagonists are known to induce the conformation of $\alpha_{IIb}\beta 3$ with high affinity for fibrinogen[14]. Crystallization in the open conformation may also have been facilitated by truncation of the integrin tailpiece, which participates in extensive interfaces that stabilize the bent $\alpha_V\beta 3$ conformation$_3$. The conformation characterized here termed ‘liganded-open’ was obtained by co-crystallization with ligand, enabling equilibration to the most favoured ligand-bound conformation before crystallization. By contrast, crystals of $\alpha_V\beta_3$ were previously formed in the bent, low-affinity conformation which we term ‘unliganded-closed’, and a ligand-mimetic antagonist was then soaked-in to obtain what we term the ‘liganded-closed’ conformation[8]. Crystal packing contacts are required for maintenance of the bent, liganded-closed conformation, because in solution addition of the same ligand to bent $\alpha_V\beta_3$ induces leg extension and conversion of the headpiece to the open conformation[3].

Ligand binding to $\alpha_{IIb}\beta_3$

Small molecule antagonists bind to a small pocket atop the integrin head formed by loops from the α_{iib} β-propeller and β_3 I domain (Figs 2a and 3a–d). The binding site for the macromolecular ligand fibrinogen is more extensive, as revealed by the positions of residues shown by mutation to affect binding (Fig. 3a). In macromolecular recognition, the β_3 specificity determining loop (SDL) and four α_{iib} β-propeller loops that form a cap subdomain are particularly important, with 71% of fibrinogen-sensitive α_{iib} mutations mapping to the latter[20]. The α_{iib}-specific 10E5 Fab binds solely to the α_{iib} cap subdomain (Fig. 2a, Supplementary Material and Supplementary Fig. 2) and has no effect on its conformation (Fig. 2b). Binding of small molecules is not blocked by 10E5, as shown by their co-crystallization (Figs 2a and 3a–d), and thus blocks binding of fibrinogen to $\alpha_{IIb}\beta 3$ (ref. 19) solely by occluding the macromolecular recognition site on the α_{iib} cap subdomain. By contrast, the β_3 specific-7E3 Fab, abciximab, blocks fibrinogen- binding by binding to residues in theβ_3 SDL[5,21].

The cap subdomain helps form the drug-binding pocket as well as the macromolecular recognition surface on α_{iib}. It is comprised of four long insertions or loops in the β-propeller domain (Supplementary Fig. 1a). Insert 3 forms an a -helix in the α_{iib} drug-binding pocket (Fig. 3a–d), and in integrina subunits that contain I domains forms the ligand-bindinga I domain[4]. Inserts 1 and 2 form a four-stranded anti-parallel β-sheet in the centre of the cap subdomain that is buttressed on one side by the α-helix and loop of insert 4, and on the other side by the β_3 SDL (Fig. 2a). Alternative splicing of cap insert 4 can regulate ligand-binding specificity[22,23].

The greatest structural differences between the α_{iib} and α_V β-propellers are in cap inserts 1, 2 and 3 (Fig. 2d). The β_3 SDL closely associates with the cap subdomain, and structural variation between α_{iib} and α_V appears to be responsible for the different β_3 SDL conformations in$\alpha_{IIb}\beta3$ and $\alpha_V\beta_3$ (Figs 2d and 3d compared with 3f). By contrast, the remainder of theα_{iib} and α_Vb-propellers are highly conserved structurally, with a root mean square deviation of 1.4Å for 391 residues. The hub of theβ-propeller that associates with the β I domain is especially conserved, enabling up to eleven diverse integrin α-subunits to bind to a singleb α-subunit[24]. At their current resolutions of 2.7Å and 3.1Å, respectively, there is no significant difference between liganded-open $\alpha_{IIb}\beta3$ and unliganded-closed $\alpha_V\beta_3$ in orientation between the β-propeller and β I domains (Fig. 2d).

All crystals reported here were formed in the presence of the physiological cations Ca^{2+} and Mg^{2+}. Three metal binding sites are present in the β_3 I domain in the drug-binding pocket[8] (Figs 2a and 3a–f). In the middle site, the MIDAS, a Mg^{2+} ion coordinates a carboxyl group present in each of the three co-crystallized ligandmimetic $\alpha_{IIb}\beta3$ antagonists (Fig. 3a–d). The cacodylate ion that is bound to form A (Fig. 3e) and form B crystals binds in the same way as the carboxyl group of the ligand-mimetics, with one oxygen coordinating the MIDAS Mg^{2+} and the other hydrogen-bonding to two backbone amides. The cacodylate may thus act as a pseudo-ligand, and stabilize the open β subunit I domain conformation similarly to pseudoligand lattice contacts that stabilize the open α subunit I domain conformation[25–27]. Ca^{2+} was assigned at the two sites adjacent to the MIDAS on the basis of Yb^{3+} soaking data and coordination chemistry (see Methods). The site distal to the β-propeller is termed adjacent to MIDAS (ADMIDAS). The site near the β-propeller is termed ligand-induced metal binding site (LIMBS). The LIMBS is occupied in the open $\alpha_{IIb}\beta3$ structure even when only a cacodylate pseudoligand is bound (Fig. 3e).

Two drugs used in prevention and treatment of coronary artery thrombosis, tirofiban and eptifibatide[5], as well as Merck compound L-739758 (Fig. 3a–d), antagonize binding of fibrinogen to $\alpha_{IIb}\beta3$. These compounds were developed as mimics of the Arg-Gly-Asp sequence that is found in a wide variety of integrin glycoprotein ligands, and the $\alpha_{IIb}\beta3$-binding sequence in fibrinogen, Lys-Gln-Ala-Gly-Asp-Val[28,29,30]. In addition to $\alpha_{IIb}\beta3$, the integrins $\alpha_V b_1$, $\alpha V\beta_3$, $\alpha_V b_5$, $\alpha_V b_6$, $\alpha_V b_8$, $\alpha_5 b_1$ and $\alpha_8 b_1$ recognize the Arg-Gly-Asp motif. Therefore, a major focus of pharmaceutical development was selective inhibition of $\alpha_{IIb}\beta3$, particularly in comparison to the closely related $\alpha_V\beta_3$ integrin. Our co-crystal structures (Fig. 3b–d), and comparison to an $\alpha_V\beta_3$-selective compound soaked into $\alpha_V\beta_3$ crystals (Fig. 3f)[8], reveal the basis for drug binding and selectivity (see Supplementary Material for details). Each drug has a basic moiety that mimics the arginine in Arg-Gly-Asp or the lysine

in the fibrinogen sequence, and a carboxyl group that mimics the aspartic acid. Selectivity for $\alpha_{IIb}\beta 3$ and $\alpha_V\beta_3$ is conferred by a longer and shorter distance, respectively, between the basic and acidic moieties of peptidomimetics (Fig. 3d, f), which can be adjusted by the constraints on the cyclic ring that bears the basic and aspartic acid residues, and the length of the basic residue side chain[28,29]. Our structures show that this is because the basic ligand-mimetic side chain must reach further into the deeper β-propeller pocket of α_{iib} to hydrogen-bond to α_{iib}-Asp 224 (Fig. 3b–d), whereas in the α_Vb-propeller the hydrogen-bonding residues Asp 150 and Asp 218 are nearer in its shallower pocket (Fig. 3f). Furthermore, Asp 218 in a_V is replaced by Phe 231 in α_{iib}, favouring contacts with longer aliphatic moieties (Fig. 3b–d, f).

A large number of snake venom disintegrins with Arg-Gly-Asp sequences have evolved to inhibit haemostasis but are not $\alpha_{iib}b_3$-selective. An unusual, $\alpha_{IIb}\beta 3$-selective disintegrin with a Lys-Gly- Asp-Trp sequence led to the development of eptifibatide[31]. The lysine with its longer aliphatic side chain than arginine confers selectivity, whereas the tryptophan confers high affinity. In an independent drug development programme, exosite substituents such as pyridyl sulphonamide were found that substantially increase affinity[30] (Fig. 3c) and that occupy the same position in the drug-binding pocket as the tryptophan residue (Fig. 3d).

Comparison to the cacodylate-bound structure (Fig. 3e) demonstrates that the drug-binding pocket in $\alpha_{IIb}\beta 3$ is rigid, with the contacting residues adopting the same conformation with or without the drugs. This helps account for high affinity, despite burial of a solvent-accessible surface area of only 300–390$Å^2$ on the three drugs.

An open, high-affinity conformation for integrin β I domains

Comparisons among unliganded-closed $\alpha_V\beta_3$, liganded-closed $\alpha_V\beta_3$ and liganded-open $\alpha_{IIb}\beta 3$ reveal the atomic basis for communication of allostery between the ligand binding site in the β_3 I domain and other integrin domains (Figs 2d and 4a, c, d, e; Supplementary Movie 1). In liganded-open $\alpha_{IIb}\beta 3$ compared with unliganded-closed $\alpha_V\beta_3$, concerted movements in the β_3 I domain occur in the ligand-binding b 1–a 1 loop, the a 1-helix, the α 1–b 2 loop, the α2-helix, the β 6–a 7 loop and the α7-helix. Movements in the ligand- and metal-binding β 1–a 1 loop are similar in both liganded structures, but greater in magnitude for the liganded-open structure than the liganded-closed structure (2.9 and 2.0Å per residue for residues 121–127, respectively) (Fig. 4a, e). A single turn of 3_{10}-helix in this loop bearing the key MIDAS and ADMIDAS residue Ser 123 moves *en bloc* in the liganded-open structure, but the lesser movement in the liganded-closed structure disrupts this 3_{10}-helix.

Extensive movements occur in theb β6–aα7 loop and the α7-helix between the liganded-open and unliganded-closed structures. The β6–α7 loop moves downward, and the α7-helix moves downward and pivots laterally, resulting in an average displacement for residues 333–352 of 5.3Å (Fig. 4a, c, e). Between the unliganded-closed and liganded-closed structures there is a movement of lesser magnitude in the β6–α7 loop; however, the movements differ in direction (Fig. 4a, e). Movement in this region of the liganded-closed

structure is therefore a consequence of strain rather than movement along the pathway towards the open conformation.

In the liganded-open compared with the unliganded-closed structure, the α1-helix moves[32] upward to accommodate movements near its beginning at the MIDAS and ADMIDAS, and near its end, that allow hybrid domain swing-out (Fig. 4a). Furthermore, a bend between the 3_{10}-helix in the β1–α1 loop and the α1-helix is straightened, and the α1-helix is lengthened by five residues, as it pivots laterally to fill-in room vacated by the β6–α7 loop (Fig. 4a, c). The position of the α1-helix in the liganded-closed structure does not resemble that in the unliganded-closed or the liganded-open structures (Fig. 4a, e), suggesting that its position is off the pathway towards the open conformation, and results from strain imposed by binding to ligand when the interface with the hybrid domain remains in the closed conformation.

Changes in metal ion coordination are closely related to loop movements in the β I domain, and are key for stabilizing its alternative conformational states (Fig. 4d). Coordination of the Met 335 backbone carbonyl in the β6–α7 loop to the ADMIDAS Ca^{2+} ion in the unliganded-closed conformation (Fig. 4d)[7] is broken in liganded-closed and Mn^{2+}-bound-closed $\alpha_V\beta_3$[8], and in liganded-open $\alpha_{IIb}\beta_3$ (Fig. 4d). Mn^{2+} activates integrins by competing with Ca^{2+} at the ADMIDAS; the much lower propensity of Mn^{2+} than Ca^{2+} for carbonyl coordination enables downward displacement of the β6–α7 loop and activation in Mn^{2+} (ref. 33). Breakage of the Met 335 coordination and the movement of the β1–α1 loop with its coordinating residues enable the large movement in position of the ADMIDAS metal between the unliganded-closed and liganded-open conformations (Fig. 4d). Additionally, small shifts in the position of the MIDAS and LIMBS metals relate to marked movements and changes in metal ion coordination of residues Asp 251, Glu 220, Asn 215 and Asp 217 (Fig. 4d). The metal ions seem to occupy similar but less strained orientations in the liganded-open compared with the liganded-closed structures, with the caveat that the resolutions are 2.7 and 3.3Å, respectively. For example, the Asp 217 side chain coordinates with the LIMBS metal ion in the liganded-open structure, instead of orienting away from it in the liganded-closed structure[8,33] (Fig. 4d). Its position in the liganded-open structure is more consistent with the function of Asp 217 in β7 as a LIMBS residue that stabilizes the high-affinity state[33].

Rearrangements in the β I domain are clearly structurally homologous to those in α I domains (Fig. 4a, b). Movements of similar directionality occur in the MIDAS metal ion, β1–α1 loop, a 1-helix, β6–α7 loop anda α7-helix[4]. Hydrophobic ratchet residues that are located one turn of 3_{10}-helix apart, stabilize alternative β6–α7 loop positions in both α I and β I domains. In contrast to the one-turn displacement in the intermediate[27] and two-turn displacement in the open α I domain conformations[25,26] (Fig. 4b), a one-turn displacement occurs in the open β I domain conformation (Fig. 4a, c). Val 340, located in an upper hydrophobic pocket in the closed conformation, moves to a lower hydrophobic pocket in the open conformation, displacing Leu 343 (Fig. 4c). Movement of the a 1-helix plays a similar part in activation of α I and β I domains by accompanying the movement of metal-coordinating residues in the β1–α1 loop; however, the greater magnitude of α1-helix movement in the β I domain is accompanied by a unique ratchet-like movement: residue Leu

134 in the a 1-helix moves laterally to occupy the upper hydrophobic pocket vacated by Val 340 (Fig. 4b).

Hybrid domain swing-out

The piston-like displacement of the β I domain a α7-helix, which connects to the hybrid domain βC strand, results in complete remodelling of the interface between these domains (Figs 4a and 5a, b; Supplementary Movie 1). The interface in the closed conformation covers 1,350Å^2 and includes at its centre hydrogen-bonding residues Tyr 110, Tyr 348 and Arg 352[7]. Upon opening not only does the α7-helix move downward, but the last two residues unwrap from the helix, including Arg 352, which reorients to the exterior of the interface. The more extended conformation at the junction betweena α7 and βC, and the straightening of the angle between α7 and βC, augment the effect of α7 displacement on hybrid domain swing-out. The more extended, end-to-end orientation between the βI and hybrid domains results in a smaller interface of about 800Å^2 (Figs 4a and 5a, b). Near its centre the interface contains Tyr 110 and Tyr 348, which adopt new hydrogen-bonding partners (Fig. 5b). Reorganization of hydrogen-bonded interfaces is the general mechanism for allosteric transitions[34]. The smaller size of the open β I/hybrid interface allows some flexibility. Relative to the closed conformation, the hybrid domain swings out 698 in crystal form A, and 57°, 59° and 61° in the three molecules in crystal form B (Fig. 2b).

Structure of an integrin PSI domain

The structure of a PSI domain in an integrin (Fig. 2a and Supplementary Fig. 3b) and comparison to that in semaphorin 4D[35] demonstrate the predicted homology of these domains in plexins, semaphorins and integrins[36], and an unexpected insertion. The buried β1 strand bearing the invariant tryptophan, and the disulphide-bonded α1- and α2-helices are well conserved, but other regions differ significantly, including the longer α3-helix (Fig. 5c, d). All three shared disulphide bonds superimpose well, and a fourth shared with integrins, plexins and the growth factor receptor MET, but not semaphorins, is also revealed (Fig. 5c, d). Chemical assignment of disulphides in the integrin β_3 PSI domain was difficult because cysteines are so closely spaced in sequence[37]; the structural data reassigns all of these disulphides, including the long-range disulphide, which was previously identified as Cys 5 to Cys 435, and is now shown to link Cys 13 to Cys 435 (Fig. 5d, e and Supplementary Fig. 3b). The long-range disulphide superimposes well with the highly conserved intradomain disulphide that links the second cysteine to the last cysteine in the PSI domain of plexins and semaphorins (Fig. 5c), and this second cysteine aligns perfectly in all PSI domains, maintaining its relationship to the third cysteine in the conservedα2-helix (Fig. 5d). These findings suggest that β_3 Cys 435 is the eighth cysteine of the PSI domain, and an integral part of the PSI domain fold. Therefore, there seems to be a nested domain insertion in the β_3 structure: the β I domain is inserted in the hybrid domain, which is in turn inserted in the PSI domain (Fig. 5e).

Superposition of four independent molecules shows that the 860Å^2 interface between the hybrid and PSI domain is rigid (Fig. 2c). Arg 93 of the hybrid domain, which is invariant in vertebrate integrins, inserts its side chain into the centre of the interface, making hydrogen

bonds to one hybrid domain residue and three different PSI domain residues (Fig. 5f). Rigidity of the interface is further supported by the nearby Cys 13-Cys 435, Cys 16-Cys 38 and Cys 26-Cys49 disulphides in the PSI domain, and the Cys 406-Cys 433 disulphide in the hybrid domain (Fig. 5f). The connection to integrin EGF-like (I-EGF) domain 1 may also be rigid, because a portion of it containing residues 437–440, including Cys 437 that is predicted to be disulphide-linked within I-EGF1[38], is present in the structure and stabilized by main-chain–side-chain and side-chain–side-chain hydrogen bonds with the PSI domain.

The human platelet alloantigen HPA-1 or Pl^A system, of great importance for neonatal alloimmune thrombocytopenia and post-transfusion purpura, corresponds to a leucine/proline polymorphism at PSI residue 33 (ref. 39). Our structure shows that the Leu 33 side chain is well exposed to solvent (Fig. 2a) on a loop of the PSI domain that is flexible and particularly long in integrins (Fig. 5c, d). Polymorphic substitution of the distally located residue Arg 93 at the hybrid/PSI interface (Fig. 5f) disrupts the HPA-1a epitope[40], demonstrating the importance of the interface for structural integrity of the PSI domain. The I-EGF1 domain also participates in the HPA-1 epitope[41], further emphasizing the tight linkage between the hybrid, PSI and I-EGF1 domains.

Allosteric mechanism for integrin activation

The structural rearrangements demonstrated here between the closed and open conformations seem to be general for all integrins. The effects of mutations designed to induce hybrid domain swing-out[9,42] (Fig. 2d), allosteric activating or inhibitory mAb that bind to the hybrid domain[10,13] (Supplementary Fig. 4), disulphide cross-links in the β6–α7 loop[43] and shortening of the α7-helix in the βI domain[44], all support the conclusion that the closed and open conformations of the integrin headpiece have low and high affinity for ligand, respectively. Furthermore, these experiments have been conducted on β_1, β_2, β_3 and β_7 integrins, demonstrating the generality of our findings. Moreover, the structural rearrangements shown here are consistent with exposure of LIBS and activation epitopes, including on the PSI domain in models of the complete integrin ectodomain (Supplementary Materials).

Our study reveals the βI/hybrid domain interface as the epicentre for quaternary structural rearrangements in integrins. A movement of about 10Å occurs at the junction between the βI domain α7-helix and the hybrid domainb C-strand that results in a 62° pivot at the βI/hybrid domain interface. The rigidly connected hybrid and PSI domains act as a mechanical lever in the upper β leg that amplifies and transmits β I domain allostery to the knee between the upper and lower β legs, resulting in a 70Å displacement at the PSI domain. Because the PSI domain is near the β knee between I-EGF1 and I-EGF2, and in the closed conformation of the headpiece the β knee is near the α-subunit knee or genu, the two legs must separate by about 70Å at their knees (Fig. 1b, c). Swing-out of the upperb leg could readily occur if it were preceded by extension at the αa and β knees (Fig. 1d to 1e to 1g). Electron microscopy studies show that below the PSI domain, the β leg is flexible in the extended conformation, whereas when the a leg extends, it adopts a single favoured orientation[3]. Interestingly, swing-out of the upper β leg might also occur in the bent conformation (Fig. 1d to 1f), because if the β subunit upper and lower legs moved as a rigid body, there would be no clash

with the α subunit, facilitating conformational equilibration, and despite the 70Å separation at the knees, the C termini of the α and β subunit ectodomains would only move apart by 15Å. Thus, adjustments in the flexible β subunit lower leg domains could allow the α and β subunit transmembrane domains to remain associated during upper leg swing-out in the bent conformation (Fig. 1d to 1f to 1g). Transmembrane domain separation could thus occur as a later event in the process of integrin activation by ligand from outside the cell (Fig. 1g to 1h), whereas transmembrane domain separation is a key early step in activation by signals from within the cell[3,16] (Fig. 1d to 1e to 1j to 1h, or Fig. 1d to 1i to 1j to 1h). In the bent $\alpha_V\beta_3$ integrin conformation, there are large, hydrophilic interfaces of 2,000Å^2 each between the headpiece and the legs, and between the α and β subunit legs[3]. The latter interface would be disrupted by upper β leg swing-out, thereby weakening that between the headpiece and the legs, and facilitating adoption of the extended integrin conformation with the open headpiece observed for liganded integrins by electron microscopy[3,6] (Fig. 1c and 1h).

Our crystal structures, together with previous structural studies on integrins[3,6–8,12,15,38], now provide a clear picture of the confor mational rearrangements in the integrin head that regulate affinity for ligand, and how conformational signals are transmitted to the leg domains. Further structures are needed to define I-EGF domains 1 and 2 in both the bent and extended conformations, the apparently unique conformation of the α subunit genu in the extended conformation[3], and how allostery is communicated between the β I and α I domains[4].

Methods

Protein expression, purification and crystallization

For details and references, see Supplementary Materials. Briefly, the soluble $\alpha_{IIb}\beta3$ headpiece encompassing residues 1–621 of α_{iib} and residues 1–472 of β_3 was expressed in CHO Lec 3.2.8.1 cells with an ACID-BASE coiled-coil clasp at the C termini, as described for soluble $\alpha_{IIb}\beta_3$[45], except that a hexahistidine tag was fused to the C terminus of β_3. The expressed protein was purified by ammonium sulphate precipitation, Ni-NTA affinity chromatography and size exclusion chromatography (Superdex 200 HR), concentrated to 1 mg ml^{21}, and treated with chymotrypsin at 25 °C for 16 h. The unclasped (coiled-coil and His_6 tag removed)$\alpha_{IIb}\beta3$ protein was collected in the flow-through of a second Ni-NTA chromatography step. The purified $\alpha_{IIb}\beta3$ was mixed with the 10E5 Fab (1:1.1 molar ratio) and the complex was purified by Superdex 200 chromatography. The complex was subjected to digestion with carboxypeptidase A and B (Calbiochem) (1:100 weight ratio) in the presence of 1 mM $ZnCl_2$ at 25 °C for 16 h. A stable protease resistant core of $\alpha_{IIb}\beta3$ was obtained and further purified by a final Superdex 200 chromatography step and stored in TBS plus calcium and magnesium, and used to obtain crystal form A. To obtain crystal form B, $\alpha_{IIb}\beta3$ fragment purified through the second Ni-NTA chromatography step was mixed with an excess of the purified fibrinogeng γ chain C-terminal domain fragment (see Supplementary Information) in the presence of 1 mM $MnCl_2$ and subjected to carboxypeptidase A and B treatment. This resulted in the same pattern of$\alpha_{IIb}\beta3$ digestion as for the 10E5 Fab complex sample; however, little of the fibrinogen domain co-purified with the $\alpha_{IIb}\beta3$ headpiece upon Superdex 200 chromatography, probably owing to hydrolysis of

the$\alpha_{IIb}\beta 3$-binding C-terminal residues of the fibrinogeng γ chain by carboxypeptidase. This material was used to obtain crystal form B, which contains no fibrinogen fragment.

The Topaz crystallizer (Fluidigm) was used to identify initial crystallization conditions by free interfacial diffusion and the lead conditions were optimized with hanging-drop vapour diffusion. The final optimized well solution for form A crystals of the 10E5 Fab: $\alpha_{IIb}\beta 3$ complex is 11% PEG 3350, 0.7 M magnesium acetate and 0.1 M sodium cacodylate, pH 6.5, and for crystal form B is 10% PEG 8000, 0.4 M magnesium acetate and 0.1 M sodium cacodylate, pH 7.0. Acetate and 4 °C temperature were absolutely required for crystallization. To obtain co-crystals with the drugs, protein sample was mixed with each drug at 1:3 to 1:5 molar ratios before setting up the hanging drops. The optimized crystallization conditions were 10–12% PEG 3350, 0.7 M magnesium acetate and 0.1 M imidazole (pH 6.5) in place of cacodylate.

Structure determination

Diffraction data were collected at the 19-ID station of the Advanced Photon Source (APS) at the Argonne National Laboratory and the A-1 station of the Cornell High Energy Synchrotron Source (CHESS). The structure of crystal form A was determined by molecular replacement using search models of theb I domain and theb I domain plus the β-propeller from $\alpha_V\beta_3$ (PDB ID 1L5G), and a murine Fab 36–71 (PDB ID 6FAB). Electron density maps calculated using phases from the search models clearly showed the presence of the hybrid domain, plus difference densities in the CDR loops of the Fab. The hybrid domain was placed in density and rebuilt. Excellent densities for landmark residues Phe 56, Pro 57, Pro 68 and Leu 69 in the first β-strand of the hybrid domain and multiple nearby disulphide bonds in the hybrid and PSI domains (Fig. 5f and Supplementary Fig. 3a) necessitated a change in the sequence-to-structure register of thisb -strand. The structure of the PSI domain was built on the basis of the electron density maps computed with refined models and guided by the secondary structure arrangements in the sema4D crystal structure[35]. Strong electron density for the conserved disulphides, the single tryptophan and the secondary structures allowed unambiguous tracing of the whole domain. Continuous electron density extends beyond residue Cys 435 and allowed the building of residues Ala 436 to Gln 440 of I-EGF1, although alternative conformations of these residues cannot be ruled out. The structure of crystal form B was solved by molecular replacement using the $\alpha_{IIb}\beta 3$ structure in crystal form A as a search model. The structures of the drug bound $\alpha_{IIb}\beta 3$ were solved by molecular replacement using the native structure as a search model. Electron density for the bound drug molecules was readily discernible in the maps calculated with the molecular replacement solution.

Supplementary Material

Refer to Web version on PubMed Central for supplementary material.

Acknowledgements

We thank colleagues in the Springer laboratory for supporting data and stimulating discussions, B. Kessler for tandem mass spectrometry, E. Yvonne Jones at Oxford for sema4D coordinates, members of the J.H.W. and M. Eck laboratories and the staff at APS and CHESS for assistance with crystallography, M. Gerstein and N. Echols (Yale

University) for the morphing script used in producing movies, and Y. Cheng for help with comparing crystal structures and the electron microscopy map. Supported by NIH grants to T.A.S., J.H.W. and B.S.C.

References

1. Hughes PE, Pfaff M. Integrin affinity modulation. Trends Cell Biol. 1998; 8:359–364. [PubMed: 9728397]
2. Takagi J, Springer TA. Integrin activation and structural rearrangement. Immunol. Rev. 2002; 186:141–163. [PubMed: 12234369]
3. Takagi J, Petre BM, Walz T, Springer TA. Global conformational rearrangements in integrin extracellular domains in outside-in and inside-out signaling. Cell. 2002; 110:599–611. [PubMed: 12230977]
4. Springer, TA.; Wang, J.-h. Cell Surface Receptors. Garcia, KC)., editor. Elsevier; San Diego: 2004.
5. Coller BS. Platelet GPIIb/IIIa antagonists: the first anti-integrin receptor therapeutics. J. Clin. Invest. 1997; 99:1467–1471. [PubMed: 9119988]
6. Takagi J, Strokovich K, Springer TA, Walz T. Structure of integrina α5β1 in complex with fibronectin. EMBO J. 2003; 22:4607–4615. [PubMed: 12970173]
7. Xiong J-P, et al. Crystal structure of the extracellular segment of integrina αVβ3. Science. 2001; 294:339–345. [PubMed: 11546839]
8. Xiong JP, et al. Crystal structure of the extracellular segment of integrina αVβ3 in complex with an Arg-Gly-Asp ligand. Science. 2002; 296:151–155. [PubMed: 11884718]
9. Luo B-H, Springer TA, Takagi J. Stabilizing the open conformation of the integrin headpiece with a glycan wedge increases affinity for ligand. Proc. Natl Acad. Sci. USA. 2003; 100:2403–2408. [PubMed: 12604783]
10. Luo B-H, Strokovich K, Walz T, Springer TA, Takagi J. Allosteric β1 integrin antibodies that stabilize the low affinity state by preventing the swing-out of the hybrid domain. J. Biol. Chem. 2004; 279:27466–27471. [PubMed: 15123676]
11. Luo B-H, Springer TA, Takagi J. High affinity ligand binding by integrins does not involve head separation. J. Biol. Chem. 2003; 278:17185–17189. [PubMed: 12600996]
12. Mould AP, et al. Structure of an integrin-ligand complex deduced from solution X-ray scattering and site-directed mutagenesis. J. Biol. Chem. 2003; 278:39993–39999. [PubMed: 12871973]
13. Mould AP, et al. Conformational changes in the integrin βA domain provide a mechanism for signal transduction via hybrid domain movement. J. Biol. Chem. 2003; 278:17028–17035. [PubMed: 12615914]
14. Du X, et al. Ligands “activate” integrina αIIbβ3 (platelet GPIIb-IIIa). Cell. 1991; 65:409–416. [PubMed: 2018974]
15. Adair BD, Yeager M. Three-dimensional model of the human platelet integrina αIIbβ3 based on electron cryomicroscopy and X-ray crystallography. Proc. Natl Acad. Sci. USA. 2002; 99:14059–14064. [PubMed: 12388784]
16. Luo B-H, Springer TA, Takagi J. A specific interface between integrin transmembrane helices and affinity for ligand. PLoS Biol. 2004; 2:776–786.
17. Vinogradova O, et al. A structural mechanism of integrina $\alpha_{IIb}\beta_3$ “inside-out” activation as regulated by its cytoplasmic face. Cell. 2002; 110:587–597. [PubMed: 12230976]
18. Kim M, Carman CV, Springer TA. Bidirectional transmembrane signaling by cytoplasmic domain separation in integrins. Science. 2003; 301:1720–1725. [PubMed: 14500982]
19. Coller BS, Peerschke EI, Scudder LE, Sullivan CA. A murine monoclonal antibody that completely blocks the binding of fibrinogen to platelets produces a thrombasthenic-like state in normal platelets and binds to glycoproteins IIb and/or IIIa. J. Clin. Invest. 1983; 72:325–338. [PubMed: 6308050]
20. Kamata T, Tieu KK, Springer TA, Takada Y. Amino acid residues in the αIIb subunit that are critical for ligand binding to integrina αIIbβ3 are clustered in theβ-propeller model. J. Biol. Chem. 2001; 276:44275–44283. [PubMed: 11557768]

21. Artoni A, et al. The specificity determining loop and α helix 1 on human integrin β3 determine the binding of murine monoclonal antigbody 7E3 toa αIIbβ3: implications for the mechanism of integrin activation. Proc. Natl Acad. Sci. USA. 2004 in the press.
22. Zavortink M, Bunch TA, Brower DL. Functional properties of alternatively spliced forms of the Drosphila PS2 integrina subunit. Cell Adhes. Commun. 1993; 1:251–264. [PubMed: 7521756]
23. von der Mark H, et al. Alternative splice variants of α7β1 integrin selectivity recognize different laminin isoforms. J. Biol. Chem. 2002; 277:6012–6016. [PubMed: 11744715]
24. Springer TA. Predicted and experimental structures of integrins and β-propellers. Curr. Opin. Struct. Biol. 2002; 12:802–813. [PubMed: 12504686]
25. Lee J-O, Rieu P, Arnaout MA, Liddington R. Crystal structure of the A domain from the α subunit of integrin CR3 (CD11b/CD18). Cell. 1995; 80:631–638. [PubMed: 7867070]
26. Lee J-O, Bankston LA, Arnaout MA, Liddington RC. Two conformations of the integrin A-domain (I-domain): a pathway for activation? Structure. 1995; 3:1333–1340. [PubMed: 8747460]
27. Shimaoka M, et al. Structures of the α L I domain and its complex with ICAM-1 reveal a shape-shifting pathway for integrin regulation. Cell. 2003; 112:99–111. [PubMed: 12526797]
28. Scarborough RM, Gretler DD. Platelet glycoprotein IIb-IIIa antagonists as prototypical integrin blockers: novel parenteral and potential oral antithrombotic agents. J. Med. Chem. 2000; 43:3453–3473. [PubMed: 10999999]
29. Gottschalk KE, Kessler H. The structures of integrins and integrin-ligand complexes: implications for drug design and signal transduction. Angew. Chem. Int. Edn Engl. 2002; 41:3767–3774.
30. Egbertson MS, et al. Non-peptide GPIIb/IIIa inhibitors. 20. Centrally constrained thienothiophene alpha-sulfonamides are potent, long acting in vivo inhibitors of platelet aggregation. J. Med. Chem. 1999; 42:2409–2421. [PubMed: 10395482]
31. Scarborough RM, et al. Design of potent and specific integrin antagonists. J. Biol. Chem. 1993; 268:1066–1073. [PubMed: 8419315]
32. Mould AP, et al. Integrin activation involves a conformational change in the α 1 helix of the β subunit A-domain. J. Biol. Chem. 2002; 277:19800–19805. [PubMed: 11893752]
33. Chen JF, Salas A, Springer TA. Bistable regulation of integrin adhesiveness by a bipolar metal ion cluster. Nature Struct. Biol. 2003; 10:995–1001. [PubMed: 14608374]
34. Perutz MF. Mechanisms of cooperativity and allosteric regulation in proteins. Q. Rev. Biophys. 1989; 22:139–237. [PubMed: 2675171]
35. Love CA, et al. The ligand-binding face of the semaphorins revealed by the high-resolution crystal structure of SEMA4D. Nature Struct. Biol. 2003; 10:843–848. [PubMed: 12958590]
36. Bork P, Doerks T, Springer TA, Snel B. Domains in plexins: Links to integrins and transcription factors. Trends Biochem. Sci. 1999; 24:261–263. [PubMed: 10390613]
37. Calvete JJ, Henschen A, González-Rodríguez J. Assignment of disulphide bonds in human platelet GPIIIa. A disulphide pattern for the β-subunits of the integrin family. Biochem. J. 1991; 274:63–71. [PubMed: 2001252]
38. Beglova N, Blacklow SC, Takagi J, Springer TA. Cysteine-rich module structure reveals a fulcrum for integrin rearrangement upon activation. Nature Struct. Biol. 2002; 9:282–287. [PubMed: 11896403]
39. Newman PJ, Derbes RS, Aster RH. The human platelet alloantigens, PlA1 and PlA2, are associated with a leucine33/proline33 amino acid polymorphism in membrane glycoprotein IIIa, and are distinguishable by DNA typing. J. Clin. Invest. 1989; 83:1778–1781. [PubMed: 2565345]
40. Watkins NA, et al. HPA-1a phenotype-genotype discrepancy reveals a naturally occurring Arg93Gln substitution in the platelet β3 integrin that disrupts the HPA-1a epitope. Blood. 2002; 99:1833–1839. [PubMed: 11861302]
41. Kunicki TJ, et al. The P1A alloantigen system is a sensitive indicator of the structural integrity of the amino-terminal domain of the human integrin β3 subunit. Blood Cells Mol. Dis. 1995; 21:131–141. [PubMed: 8846042]
42. Chen JF, et al. The relative influence of metal ion binding sites in the I-like domain and the interface with the hybrid domain on rolling and firm adhesion by integrina α4β7. J. Biol. Chem. in the press.

43. Luo B-H, Takagi J, Springer TA. Locking the β3 integrin I-like domain into high and low affinity conformations with disulfides. J. Biol. Chem. 2004; 279:10215–10221. [PubMed: 14681220]
44. Yang W, Shimaoka M, Chen JF, Springer TA. Activation of integrin β subunit I-like domains by one-turn C-terminala α-helix deletions. Proc. Natl Acad. Sci. USA. 2004; 101:2333–2338. [PubMed: 14983010]
45. Takagi J, Erickson HP, Springer TA. C-terminal opening mimics "inside-out" activation of integrina α5β1. Nature Struct. Biol. 2001; 8:412–416. [PubMed: 11323715]
46. Esnouf RM. An extensively modified version of MolScript that includes greatly enhanced coloring capabilities. J. Mol. Graph. Model. 1997; 15:132–138. [PubMed: 9385560]
47. Merritt EA, Murphy MEP. Raster 3D version 2.0: a program for photorealistic graphics. Acta Crystallogr. D. 1994; 50:869–873. [PubMed: 15299354]
48. Carson M. Ribbons. Methods Enzymol. 1997; 277:493–505. [PubMed: 18488321]
49. Puzon-McLaughlin W, Kamata T, Takada Y. Multiple discontinuous ligand-mimetic antibody binding sites define a ligand binding pocket in integrina αIIbβ3. J. Biol. Chem. 2000; 275:7795–7802. [PubMed: 10713093]
50. Tozer EC, Liddington RC, Sutcliffe MJ, Smeeton AH, Loftus JC. Ligand binding to integrin$\alpha_{IIb}\beta 3$ is dependent on a MIDAS-like domain in the β3 subunit. J. Biol. Chem. 1996; 271:21978–21984. [PubMed: 8703003]

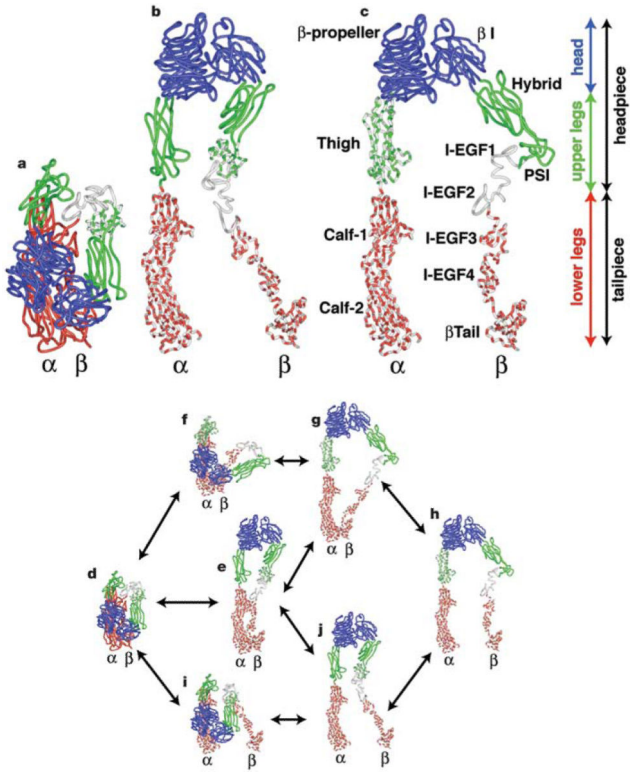

Figure 1.

Quaternary rearrangements in the integrin ectodomain. **a–c**, Three conformational states visualized in electron microscopy[3,6] and in crystal structures (here and in ref. 7). **d–j**, Proposed intermediates in equilibration between known conformational states. The upper pathways may be stimulated by ligand binding outside the cell, and the lower pathways by signals within the cell that separate the α and β subunit transmembrane domains. Domains in **a–j** are shown in solid colour if known directly from crystal structures, dashed with grey if placed from crystal structures into electron microscopy image averages, and in solid grey for EGF-1 and EGF-2, which are modelled on EGF-3 and EGF-4.

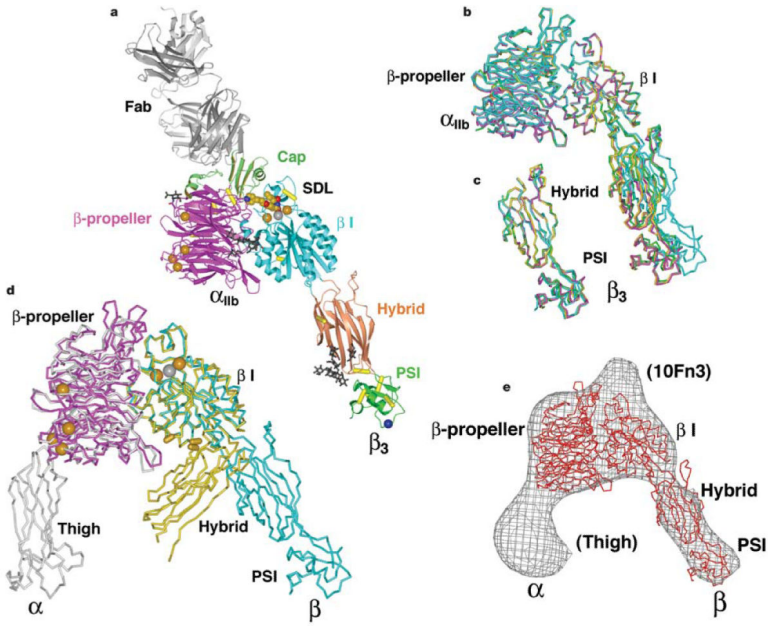

Figure 2.

Structure of the $\alpha_{IIb}\beta 3$ headpiece. **a**, Ribbon diagram of the $\alpha_{IIb}\beta 3$:10E5 complex. Calcium and magnesium ions are shown as gold and silver spheres, respectively. Tirofiban is shown in cpk. The Cα atom of HPA-1a alloantigenic determinant Leu 33 in the PSI domain is shown as a blue sphere. Glycan chains are displayed as black sticks. Integrin disulphides are shown as yellow Cα –Ca bonds. **b**, Superimposed on the basis of the β I domain are the three independent $\alpha_{IIb}\beta 3$ heterodimers in crystal form B (magenta, green and yellow), and one in form A (cyan). **c**, The hybrid and PSI domains of the four independent $\alpha_{IIb}\beta 3$ structures are superimposed. **d**, Liganded-open $\alpha_{IIb}\beta 3$ (crystal form A) and unliganded-closeda $\alpha_V\beta_3$ headpieces[7] are superimposed using the β I domainb -sheet. The α and β subunits are coloured magenta and cyan in $\alpha_{IIb}\beta 3$ and grey and yellow in $\alpha_V\beta_3$. Calcium and magnesium ions in$\alpha_{IIb}\beta 3$ only are gold and silver spheres, respectively. Yellow cylinders in the β I/hybrid interface show positions of residues where introduction of N-glycosylation sites induces high affinity for ligand and LIBS epitope exposure[9,42]. **e**, Superposition of an $\alpha_{IIb}\beta 3$ structure from crystal form B (red Cα-trace) on the three-dimensional electron microscopy density (grey chickenwire) of the fibronectin-bounda $\beta_5\beta_1$ headpiece[6]. Domains are labelled and those only in the $\alpha_5 b_1$ structure including the tenth FN3 domain of fibronectin are in parentheses. Figures in this paper utilize crystal form A unless stated otherwise and were prepared with programs Bobscript[46], Povray (The Povray Team, http://www.povray.org), Raster3D[47] and Ribbons[48].

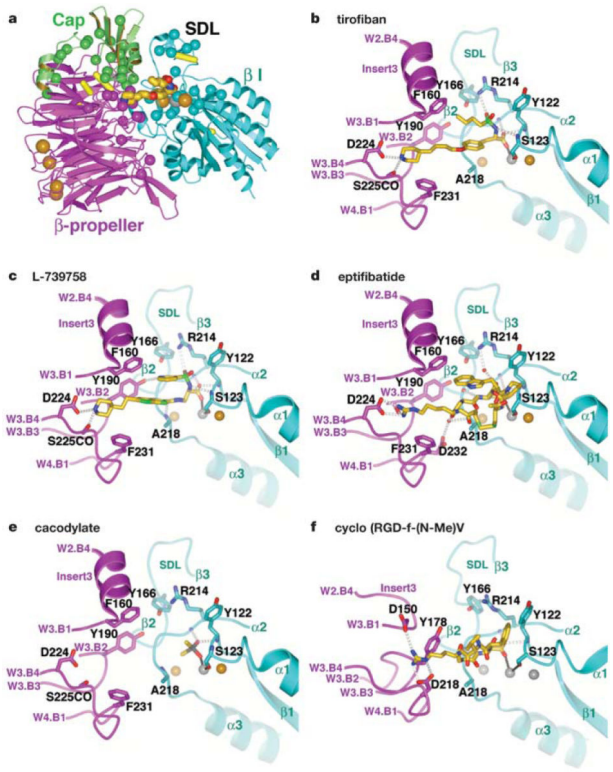

Figure 3.

The binding sites for ligand-mimetic antagonists and fibrinogen at the α/β subunit interface. **a**, Mapping of fibrinogen binding sensitive mutations[20,49,50] in $\alpha_{IIb}\beta 3$. Cβ atoms of fibrinogen-binding sensitive residues are shown as spheres in the same colour as the domains in which they are present. The tirofiban-bound structure is shown. **b–f**, Binding of ligands or pseudoligands to $\alpha_{IIb}\beta 3$ (**b–e**) and binding of (**f**) cyclo Arg-Gly-Asp-D-Phe-N-methyl-Val (cyclo RGDfV) to $\alpha_V\beta_3$ (ref. 8). The orientation is identical to that in **a**. The α and β subunits are shown in magenta and cyan, respectively. Small molecules are shown as ball-and-stick models with their carbon, nitrogen, oxygen, sulphur and arsenic atoms coloured yellow, blue, red, green and grey, respectively. Hydrogen bonds are shown as dotted lines. Ca^{2+} and Mg^{2+} ions are gold and silver spheres, respectively. The ligand and S123 coordinations to the MIDAS metal are shown as thin grey lines.

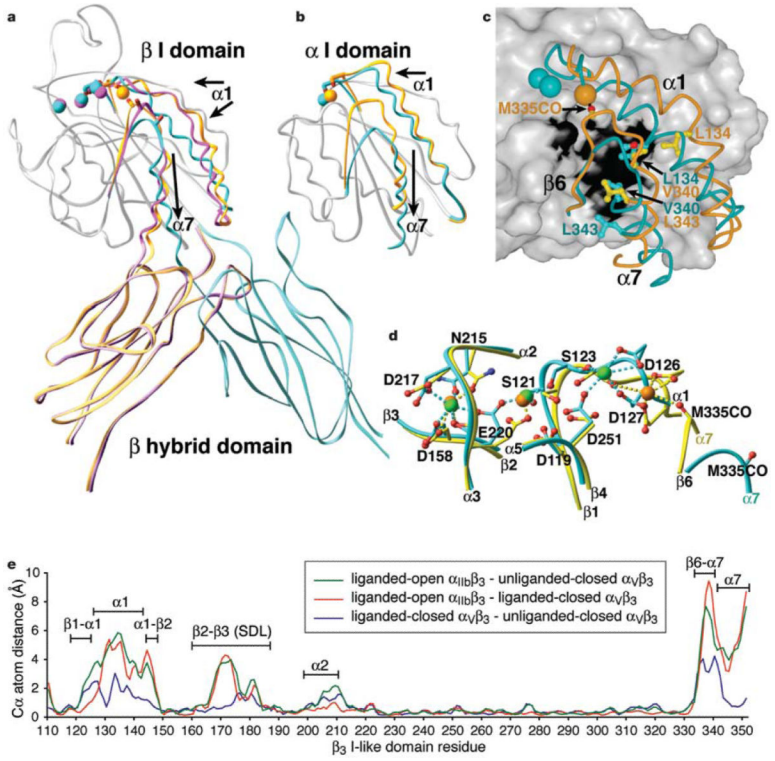

Figure 4.

Allostery in theb I domain and comparison with α I domain. **a**, Overview of motions in the β_3 I and hybrid domains. Non-moving parts of the backbone are shown as a grey worm. Moving segments shown as Cα-traces are from unliganded-closed $\alpha_V\beta_3$ (gold), liganded-closed $\alpha_V\beta_3$ (magenta) and liganded-open $\alpha_{IIb}\beta3$ (cyan). The direction of movement is shown with arrows. **b**, Comparison witha I domains. The moving segments of unliganded-closed (gold) and pseudoliganded-open (cyan) α_M I domains[25,26] and their MIDAS metal ions are shown as in **a** and in the same orientation. **c**, Hydrophobic ratchet pockets underlying the β6–α 7 loop anda 1-helix. The unliganded-closed (orange) and liganded open (cyan) β 1–α 1 loop, α 1-helix, α 1–b 2 loop and β 6–α 7 loop anda 7-helix are shown as worm traces with key side chains, the Met 335 carbonyl and metal ions in the same colour. The rest of the domain is shown as a grey surface, except for hydrophobic pocket residues Tyr 116, Val 247, Thr 249, Ile 307, Ala 309 and Thr 311, which are shown as a black surface. **d**,β_3 I domain metal coordination sites in liganded-open $\alpha_{IIb}\beta3$ (cyan) and unliganded-closed $\alpha_V\beta_3$ (yellow). LIMBS, MIDAS and ADMIDAS positions are shown left to right in similar orientation as in a. The LIMBS and MIDAS were not occupied in the unliganded-closed structure[7]; for reference, metal ions at these sites are shown from the liganded-closed structure[8]. In **a–d**, metal ions are shown as spheres in the same or a similar (**d**) colour as their associated backbone. **e**, Distances between Ca atoms in the three superimposed β I domains, smoothed by averaging at each residue over a 3-residue window.

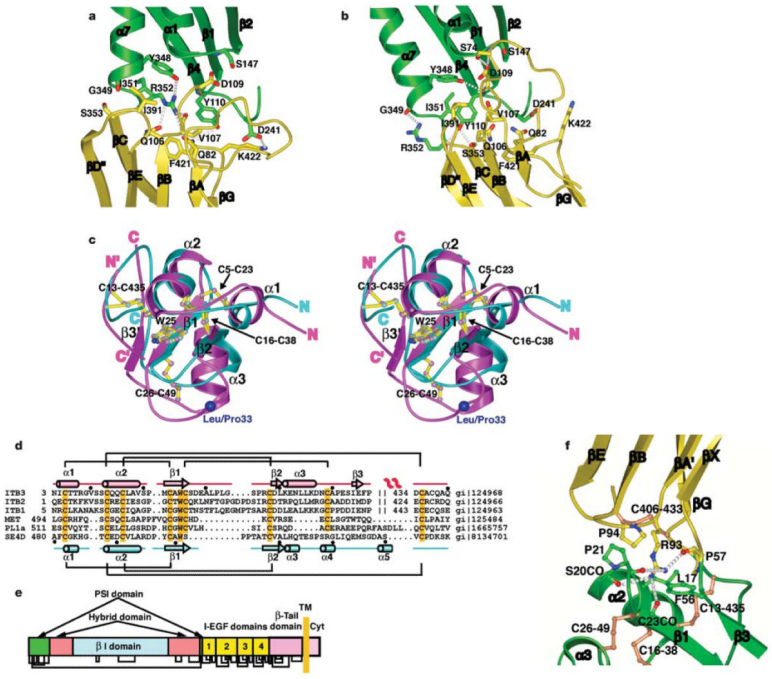

Figure 5.

The hybrid and PSI domains and their interfaces. **a**, **b**, The β I/hybrid domain interface in the unliganded-closed structure[7] (**a**) and liganded-open structure (**b**). Ribbon backbone and side-chain carbon atoms are shown in green (β I) and yellow (hybrid) with theb I domainb β-sheet in the same orientation. The α7-helical ribbon is shown up to the same residue (350) in both structures to aid comparison of α7-helix position. **c**, Stereo view of the superposition of the PSI domains fromβ_3 (magenta) and semaphorin4D (cyan). The disulphide bridges and the conserved tryptophan are shown as ball-and-stick models with their bonds coloured yellow and atoms the same colour as the backbone. The Leu/Pro 33 alloantigen site is represented with a large blue Ca sphere. The amino and carboxyl termini of each domain are indicated. The N' and C' refer to termini for residues 434–440 that constitute part of the PSI and EGF-1 domains. **d**, Sequence alignment of PSI domains from integrins, semaphorin4D (SE4D), a plexin and c-met. Disulphide connections are shown above (β_3) and below (semaphorin4D) the respective sequences. The conserved cysteines and tryptophans are highlighted orange. The secondary structures are shown for β_3 (top) and sema4D (bottom). **e**, Domain organization of integrin β subunits, showing multiple domain insertions. The revised disulphide bond pattern is shown below. **f**, The interface between the hybrid (yellow) and PSI (green) domains. Disulphide bonds are shown in orange.